THE JOURNAL OF PHYSICAL CHEMISTRY A

Article

pubs.acs.org/JPCA

Primary Product Branching in the Photodissociation of Chloroacetaldehyde at 157 nm

Jonathan D. Adams, Preston G. Scrape, Shenshen Li, Shih-Huang Lee,[†] and Laurie J. Butler*[,‡]

[†]National Synchrotron Radiation Research Center, Hsinchu 30076, Taiwan, Republic of China

[‡]The James Franck Institute, Department of Chemistry, The University of Chicago, Chicago, Illinois 60637, United States

Supporting Information

ABSTRACT: We used crossed laser-molecular beam scattering to study the primary photodissociation channels of chloroacetaldehyde (CH_2ClCHO) at 157 nm. In addition to the C−Cl bond fission primary photodissociation channel, the data evidence two other photodissociation channels: HCl photoelimination and C−C bond fission. This is the first direct evidence of the C−C bond fission channel in chloroacetaldehyde, and we found that it significantly competes with the C−Cl bond fission channel. We determined the total primary photodissociation branching fractions for C−Cl fission:HCl elimination:C−C fission to be 0.65:0.07:0.28. The branching between the primary channels suggests the presence of interesting excited state dynamics in chloroacetaldehyde. Some of the vinoxy radicals from C−Cl photofission and most of the ketene cofragments formed in HCl photoelimination have enough internal energy to undergo secondary dissociation. While our previous velocity map imaging study on the photodissociation of chloroacetaldehyde at 157 nm focused on the barrier for the unimolecular dissociation of vinoxy to H + ketene, this work shows that the HCl elimination channel contributed to the high kinetic energy portion of the m/z = 42 signal in that study.

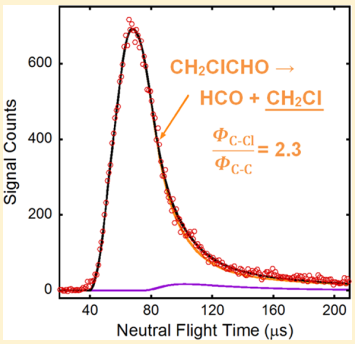

1.0. INTRODUCTION

Chloroacetaldehydes are intermediates in the degradation of chlorinated alkanes and alkenes, and they are of interest in atmospheric chemistry. Monochloroacetaldehyde has been detected as an intermediate in the oxidative degradation of 1,3-dichloropropene[1] and is a major product in the OH-initiated oxidation of ethyl chloride and 1,2-dichloroethane, which is used in the production of vinyl chloride.[2,3] Photolysis and reaction with OH radicals and Cl atoms are the primary loss channels for chloroacetaldehydes, determining the atmospheric lifetime of these species.[3] While the kinetics of the chloroacetaldehydes have been studied in great detail, few studies have been done on their photodecomposition, and therefore, little is known about the primary photodissociation pathways. Such studies can provide insight into the excited-state dynamics of the chloroacetaldehydes and provide information not only on the species released into the atmosphere by photolysis of the chloroacetaldehydes but also the relative amounts of the species if the branching between the primary channels can be determined. Therefore, characterizing the photodissociation processes of chloroacetaldehyde provides useful information for modeling atmospheric systems.

In a previous study on the photodissociation of chloroacetaldehyde at 193 nm, Miller et al.[4] observed two primary channels: a major C−Cl bond fission and a minor HCl elimination channel with a 27:1 branching ratio. At 157 nm, there have been no prior studies of the primary photodissociation channels. One might expect C−Cl photofission to dominate because one can reach excited states repulsive along the C−Cl bond at 157 nm. However, our prior study of the dissociation channels of vinoxy radicals produced from the 157 nm photodissociation of chloroacetadehyde found evidence for high recoil kinetic energy ketene cofragments formed in HCl elimination.[5] Most of the ketene products detected were from the unimolecular dissociation of highly vibrationally excited vinoxy radicals, in part because it is possible for ketene cofragments from HCl photoelimination to undergo secondary dissociation. To assess the branching to the HCl photoelimination channel, one must thus detect the HCl photofragments. We do so in this work.

One might not a priori expect C−C photofission to be important when chloroacetaldehyde is excited at 157 nm, but upon excitation at lower energies, C−C bond photofission has been observed in related molecules. Photofission of the C−C bond was observed in the photodissociation of chloroacetone at 308[6,7] and 193 nm.[8] It has also been hypothesized in the photochemistry of other chlorocompounds.[9] The UV absorption spectra of chloroacetone[10] and chloroacetaldehyde[4] in the region from 230 to 340 nm both have a broad absorption band peaking near 308 nm, assigned to the $n(O) \rightarrow \pi^*(C{=}O)$ transition. The VUV absorption spectrum of chloroacetaldehyde has been reported,[11] and the electronic assignments for the spectral features involve the Cl and C=O chromophores. Preliminary measurements in our laboratory evidenced a C−C

Received: May 31, 2017
Revised: July 31, 2017

DOI: 10.1021/acs.jpca.7b05318
J. Phys. Chem. A XXXX, XXX, XXX−XXX

photofission channel at 193 nm, so we were motivated to investigate the possibility of this channel at 157 nm in this work.

This paper reports our study of the photodissociation channels of chloroacetaldehyde at 157 nm done at the National Synchrotron Radiation Research Center (NSRRC) in Hsinchu, Taiwan. Tunable VUV photoionization reduces dissociative photoionization and allows for the detection of fragments that have high ionization thresholds such as Cl (12.97 eV[12]) and HCl (12.74 eV[12]) using single-photon photoionization. Measuring the velocity distribution of the products aids in assigning the signal from each photoproduct channel. The known photoionization cross sections of Cl atoms and HCl allow us to quantify the branching fractions to C−Cl photofission and HCl photoelimination, while our recent measurement[13] of the photoionization cross section of CH_2Cl allows us to quantify the branching to C−C photofission. The study also allows us to characterize the small contribution of ketene from HCl photoelimination to the m/z = 42 signal observed in our prior study[5] of the dissociation of vinoxy to H + ketene.

2.0. METHODS

2.1. NSRRC Scattering Apparatus. The data presented in this section were taken at the National Synchrotron Radiation Research Center (NSRRC) in Hsinchu, Taiwan using the U9 Chemical Dynamics Beamline and a crossed laser-molecular beam scattering apparatus. The apparatus has been described in detail elsewhere;[14−16] we provide a brief description here. A 3% molecular beam of chloroacetaldehyde was created by first seeding the vapor pressure at 25 °C of the liquid sample (50% solution in water from Sigma-Aldrich, used without further purification) in neon with a total backing pressure of ∼600 Torr. The gaseous mixture was then supersonically expanded into a rotating source chamber through a pulsed nozzle with a 0.25 mm orifice. The nozzle was operated at 100 Hz and held at a temperature of 60 °C. The rotating source was set at an angle of 10° or 20° with respect to the detection axis. The molecular beam intersected the 157 nm unpolarized output of a LPF 200 Lambda Physik Laser Technik laser propagating perpendicularly to the plane created by the molecular beam and the detector axis. The beam was focused to an area of ∼2.5 × 8 mm^2 at its intersection with the molecular beam, and the pulse energy was maintained near 8 mJ.

Following photodissociation, the resulting fragments recoil with a range of net velocities representing the vector sum of the recoil velocities (from both primary photofission and secondary dissociation of a portion of fragments formed with high internal energy) and the velocity of the precursor in the molecular beam. Those fragments with a net velocity vector pointing into the detector traveled 10.05 cm to the ionizer region, where they were ionized by tunable VUV synchrotron radiation. Photoionization energies were chosen by tuning the U9 undulator gap, and the input undulator radiation was defined by a 7 mm diameter circular aperture. Higher harmonics of the VUV radiation were filtered out using a 30 cm gas cell containing ∼10 Torr argon. The filtered undulator radiation was focused into an area of diameter ∼1 mm in the ionizer. The ionized fragments were then accelerated by a series of ions lenses through a quadrupole mass filter and counted by a Daly detector. The data reported herein were taken with a mass resolution lower than that in our previous studies at the NSRRC, so evidence, for example, a contribution at m/z = 35 signals a mass unit higher. These contributions were identified by their velocity distributions. A multichannel scaler recorded the signal count as a function of total time-of-flight (TOF), which is the sum of the flight time of the neutral fragments to the ionizer and the flight time of the ionized fragments through the detector. The neutral flight time is recovered from the total TOF by subtracting the ion flight time calculated using the calibrated ion flight coefficient of 5.43 μs $amu^{-1/2}$. The data were collected with 1 μs bins, and the times-of-flight were corrected to account for the measured 1.1 μs electronic delay between the laser and the triggering of the multichannel scaler. All TOF spectra in this paper show the neutral flight time.

The TOF spectra were fit to recoil kinetic energy distributions ($P(E_T)s$) by forward convolution fitting using the CMLAB2 program.[17] The molecular beam velocity was characterized using a photodepletion (hole-burning) technique. By operating the photolysis laser at 50 Hz and the pulsed nozzle at 100 Hz, only half of all molecular beam pulses underwent photodissociation. These measurements were taken with the rotating source chamber set on-axis with the detector. Subtracting the laser-off signal from the laser-on signal produced a hole-burned TOF spectrum from which we determine the velocity distribution of the molecules in the molecular beam that were photodissociated. The velocity distribution typically had a maximal probability at 800 m/s and a full width at half-maximum of 270 m/s (see Supporting Information).

2.2. Computational Methods. We calculated minima and transition states relevant to the primary dissociation of chloroacetaldehyde and dissociation of subsequent photoproducts with the G4 protocol. Optimized molecular geometries and vibrational frequencies were found using the B3LYP density functional and the 6-311++G(3df,2p) basis set. The geometries converged to a root-mean-square (rms) force below 1×10^{-5} and an rms displacement below 4×10^{-5}, where both values are in atomic units. Wave functions for doublet species were spin-unrestricted, and wave functions for singlet species were spin-restricted. The computation of the zero-point vibrational energies used the B3LYP/6-311++G(3df,2p) vibrational frequencies scaled by 0.9854[18] as the G4 method required.[19] The G4 method is the latest in the series of Gn theories, which are composite methods based on a sequence of single-point energy calculations. To confirm the calculated transition states lead to the desired products, we also ran an intrinsic reaction coordinate (IRC) calculation at the B3LYP/6-311++G(3df,2p) level. The calculations use the Gaussian09 program, version A.02.[20]

3.0. RESULTS

In the following sections, we present the scattering data for the photodissociation of chloroacetaldehyde with forward convolution fits. We begin with an overview of the primary photodissociation channels of chloroacetaldehyde observed in this study and the energetics of those channels. In Section 3.2, we present the TOF spectra of the primary photodissociation products from C−Cl bond fission and HCl photoelimination, taken at m/z = 35 (Cl^+), m/z = 36 ($H^{35}Cl^+$), and m/z = 38 ($H^{37}Cl^+$). For comparison to the previous chloroacetaldehyde study,[5] we characterize the contribution of stable ketene products from HCl photoelimination to the m/z = 42 TOF spectrum as well. Section 3.3 presents TOF spectra for the products from primary C−C bond photofission, taken at m/z = 29 (HCO^+) and m/z = 49 (CH_2Cl^+). The estimates of the

DOI: 10.1021/acs.jpca.7b05318
J. Phys. Chem. A XXXX, XXX, XXX−XXX

branching ratios between the three primary photodissociation channels are then described in Section 3.4. While we did observe evidence of secondary dissociation of the primary photodissociation products (at m/z = 14, 15, 28, and 42), we report the analysis of those channels elsewhere.[21]

3.1. Overview of Primary Photodissociation Channels of Chloroacetaldehyde. In the current study, we observed 3 primary photodissociation channels of chloroacetaldehyde using 157 nm photons (eqs 1−3): C−Cl bond fission producing vinoxy radicals, HCl photoelimination producing ketene, and C−C bond fission producing CH_2Cl and HCO radicals. This study provides the first direct evidence of a C−C bond fission channel.

$$CH_2ClCHO + h\nu$$

$$\rightarrow CH_2CHO + Cl \quad \Delta H_{0K} = 73.4 \text{ kcal/mol} \quad (1)$$

$$\rightarrow CH_2CO + HCl \quad \Delta H_{0K} = 7.43 \text{ kcal/mol} \quad (2)$$

$$\rightarrow HCO + CH_2Cl \quad \Delta H_{0K} = 77.2 \text{ kcal/mol} \quad (3)$$

Because the primary processes impart a range of translational energies, the products from the primary photodissociation channels are formed with a range of internal energies. Comparing the internal energy of the products to the barriers along their ground state potential energy surface (PES) and accounting for conservation of angular momentum[21] shows that some of the products from the photodissociation have enough internal energy to undergo unimolecular dissociation. From conservation of energy, the internal energy, E_{int}(A) of a product, A, formed from the photodissociation of a precursor A−B is given by the equation:

$$h\nu + E_{int}(AB) = \Delta H_{0K} + E_T + E_{int}(A) + E_{int}(B) \quad (4)$$

where $h\nu$ is the energy of the photon, E_{int}(AB) is the internal energy of the precursor, E_T is the recoil translational energy imparted to the fragments, and E_{int}(B) is the internal energy of the cofragment to A. Supersonic expansion of the molecular beam cools the rotational energy of the precursor, so E_{int}(AB) is the thermal vibrational energy at the nozzle temperature of 60 °C, which is 1.45 kcal/mol. The values of ΔH_{0K} for the primary photodissociation channels are given in eqs 1−3 and were calculated at the G4//B3LYP/6-311++G(3df,2p) level of theory. E_{int}(B) is discussed in the relevant sections below, where B represents either Cl, HCl, or CH_2Cl.

3.2. C−Cl Bond Fission and HCl Elimination. Due to the resolution of the quadrupole, we detected m/z + 1 ion signal in the TOF spectra taken at m/z for the primary photodissociation products of C−Cl bond fission and HCl photoelimination. We therefore analyzed all of the data at the mass-to-charge ratios for these channels collectively and present the analysis of both channels together in this section. We observed signal at m/z = 35 (Cl^+) corresponding to C−Cl bond fission. The presence of the HCl photoelimination channel was confirmed by detecting signal at both m/z = 36 ($H^{35}Cl^+$) and m/z = 38 ($H^{37}Cl^+$). Because the data taken at m/z = 38 ($H^{37}Cl^+$) cannot have any "bleed in" from m/z + 1 ion signal (as there is no product that gives signal at m/z = 39), we determined the P(E_T) for all HCl photoelimination events from the TOF spectrum taken at this mass-to-charge ratio. Figure 1 shows the TOF spectrum collected at m/z = 38 ($H^{37}Cl^+$) with a source angle of 10° and ionization energy of 15 eV. The experimental data are shown in red open circles and are fit using a forward-convolution method. The fit

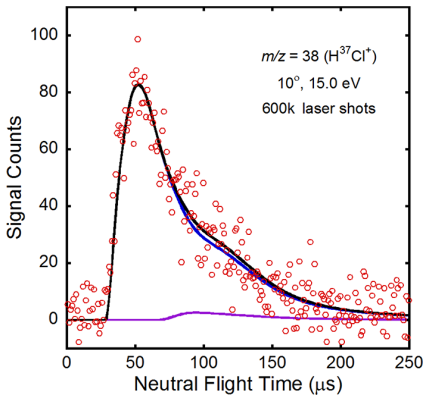

Figure 1. TOF spectrum taken at m/z = 38 ($H^{37}Cl^+$) with a source angle of 10° and an ionization energy of 15.0 eV. Data are shown in red circles. Primary HCl photoelimination is fit by the solid blue line using the P(E_T) shown in Figure 2. The contribution attributed to photodissociation of clusters in the molecular beam is shown by the solid purple line.

corresponding to primary HCl photoelimination is depicted by the solid blue line and was derived from the P(E_T) depicted by the solid blue line in Figure 2. The P(E_T) peaks at

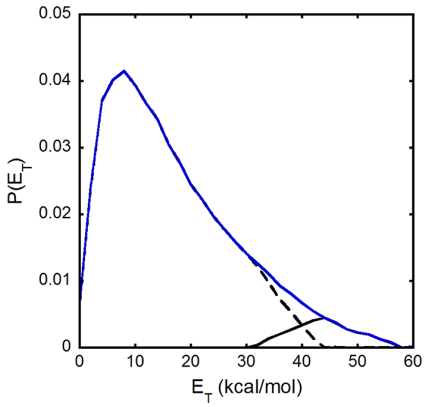

Figure 2. Photofragment recoil kinetic energy distribution for HCl photoelimination in chloroacetaldehyde at 157 nm. The total P(E_T) (solid blue line), peaking at 8 kcal/mol, is derived by forward convolution fitting of the signal at m/z = 38 ($H^{37}Cl^+$) shown in Figure 1. The portion of the P(E_T) producing stable ketene, which does not have enough internal energy to undergo secondary dissociation, is shown by the solid black line and is derived from the signal at m/z = 42 (CH_2CO^+) unfit by secondary dissociation of vinoxy. The remaining portion of the P(E_T), shown by the dashed black line, represents the portion of HCl photoelimination events that produces unstable ketene that undergo subsequent unimolecular dissociation.

8 kcal/mol and has a tail that extends to 60 kcal/mol. The contribution to the TOF spectra in Figure 1 shown by the solid purple line is from the dissociation of molecular clusters in the beam; it is characterized by an identical and slow velocity distribution seen at several m/z values.

We then determined the P(E_T) for all C−Cl bond fission events from fitting the TOF spectrum taken at m/z = 35 (Cl^+). Figure 3 shows the TOF spectrum collected at m/z = 35 (Cl^+) with a source angle of 20° and ionization energy of 13.68 eV. The experimental data are shown in open red circles. The fit shown by the solid blue line corresponds to bleed in from the

DOI: 10.1021/acs.jpca.7b05318
J. Phys. Chem. A XXXX, XXX, XXX−XXX

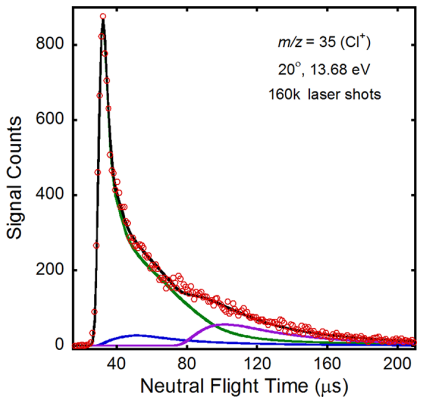

Figure 3. TOF spectrum taken at m/z = 35 (Cl^+) with a source angle of 20° and an ionization energy of 13.68 eV. Data are shown in red circles. Primary C−Cl bond fission is fit by the solid green line using the P(E_T) shown in Figure 4. The contribution from bleed in of m/z = 36 ($H^{35}Cl^+$) is shown by the solid blue line and is fit using the primary HCl photoelimination P(E_T) shown in Figure 2. The fit shown as the solid purple line represents the contribution attributed to photodissociation of clusters in the molecular beam.

m/z = 36 ($H^{35}Cl^+$) data and was calculated using the P(E_T) for HCl photoelimination shown in Figure 2. The fit corresponding to C−Cl bond fission is shown by the solid green line and was derived from the P(E_T) in Figure 4. For comparison, the

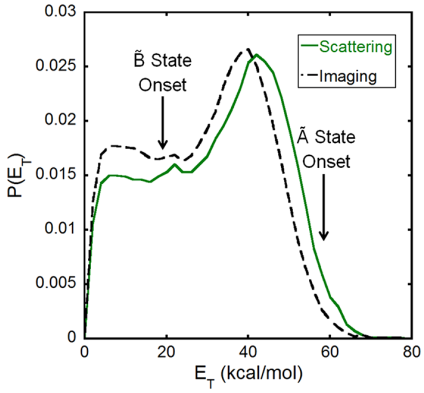

Figure 4. Photofragment recoil kinetic energy distribution for C−Cl bond fission in chloroacetaldehyde at 157 nm. The P(E_T) shown by the solid green line is derived by forward convolution fitting of the signal at m/z = 35 (Cl^+) shown in Figure 3. For comparison, the C−Cl bond fission P(E_T) derived from the velocity map imaging study (ref 5) is shown by the dashed black line. The arrows show the thresholds for producing vinoxy radicals in the Ã and B̃ excited states; these thresholds were calculated in our prior work[5] by accounting for the rotational energy that would be imparted to the vinoxy radical during C−Cl bond fission at each recoil kinetic energy.

C−Cl bond fission P(E_T) derived from the velocity map imaging study is also shown in Figure 4 by the dashed black line. While the two P(E_T)s have similar shapes, it appears that there are more dissociation events with higher kinetic energies observed in this study. The difference is within the resolution of the two apparatuses (the resolution at these energies is ∼1 kcal/mol in our velocity map imaging apparatus and 2 kcal/mol in the scattering apparatus at the NSRRC).[22,23] The high kinetic energy feature in the P(E_T) derived in this study peaks at about 42 kcal/mol. We did not observe any stable vinoxy radicals at m/z = 43 (vinoxy radicals are known to give negligible signal at parent ion upon photoionization[24]), but signals from dissociative ionization of stable vinoxy radicals formed in high kinetic energy C−Cl bond photofission events are observed in the TOF spectra taken at m/z = 15 (CH_3^+) and m/z = 29 (HCO^+). We also note that the fitting is consistent among all of the m/z = 35 (Cl^+) data, shown in Figure 5, taken

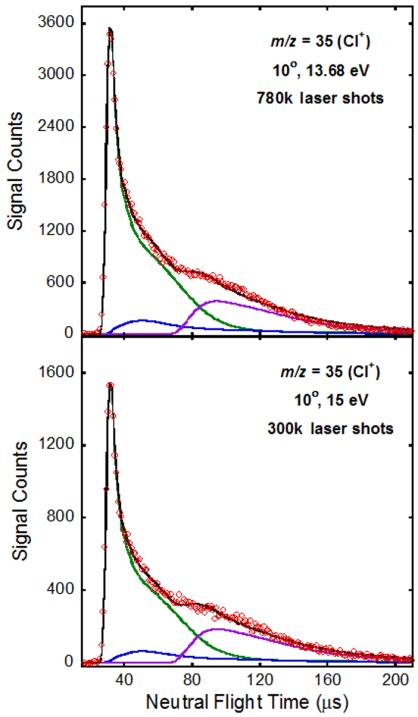

Figure 5. TOF spectrum taken at m/z = 35 (Cl^+) with a source angle of 10° and two different ionization energies. The upper frame shows the data taken at an ionization energy of 13.68 eV, and the lower frame shows the data taken at an ionization energy of 15.0 eV. Data are shown in red circles. Primary C−Cl bond fission is fit by the solid green line using the P(E_T) shown in Figure 4. The contribution from bleed in of m/z = 36 ($H^{35}Cl^+$) is shown by the solid blue line and is fit using the primary HCl photoelimination P(E_T) shown in Figure 2. The fit shown as the solid purple line represents the contribution attributed to photodissociation of clusters in the molecular beam.

at a different source angle and at different ionization energies. In the calculation of the branching ratios between the primary channels, we use the C−Cl bond fission P(E_T) derived in this study. We show alternative fits for the m/z = 35 and 36 using the C−Cl bond fission P(E_T) derived in the velocity map imaging study in the Supporting Information.

One final thing to consider is the momentum-matched ketene products from HCl photoelimination. Figure 6 shows the TOF spectrum collected at m/z = 42 (CH_2CO^+) with a source angle of 10° and a photoionization energy of 10.5 eV. The fit corresponding to the secondary dissociation of vinoxy is shown by the dashed green line and was derived using the predicted portion of the primary C−Cl bond fission P(E_T) producing vinoxy that dissociates to H + ketene from our branching calculations[5] shown in Figure 7 (see Supporting Information for further details on the branching calculations). Because we previously found a barrier height of 44.6 kcal/mol

DOI: 10.1021/acs.jpca.7b05318
J. Phys. Chem. A XXXX, XXX, XXX−XXX

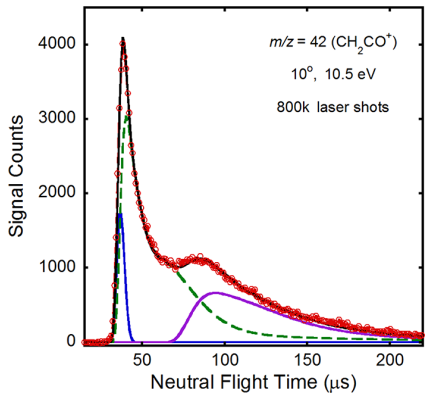

Figure 6. TOF spectrum taken at m/z = 42 (CH_2CO^+) with a source angle of 10° and an ionization energy of 10.5 eV. Data are shown in red circles. The dashed green fit shows the contribution from the dissociation of vibrationally hot vinoxy to H + CH_2CO and is calculated from the recoil translational energy of the vinoxy fragment (shown by the dashed red line in Figure 7) and from the P(E_T,2°) in Figure 8 using an isotropic angular distribution. The contribution from stable ketene produced by HCl photoelimination is shown by the solid blue and is derived from the high kinetic energy portion of the P(E_T) in Figure 2 shown by the solid black line. The fit shown by the solid purple line is the contribution from clusters in the molecular beam.

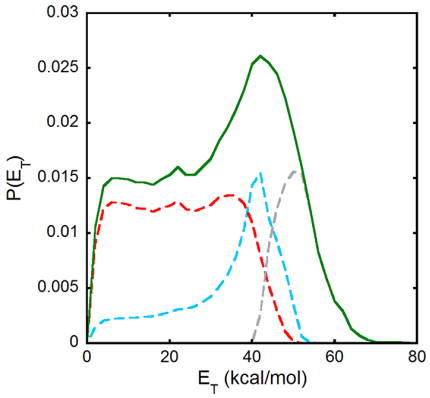

Figure 7. Results of the branching calculations described in ref 21 using a barrier height of 44.6 kcal/mol for the H loss channel. The total primary C−Cl bond fission P(E_T) derived from the scattering data is shown by the solid green line along with the predicted portions that produce H + ketene products (dashed red curve), methyl + CO products (dashed blue curve), and stable vinoxy radicals that do not dissociate (dashed gray curve). The stable portion of the P(E_T) is the distribution of C−Cl photofission events that our model predicts partitions insufficient vibrational energy to the momentum-matched vinoxy radicals to surmount the lowest barrier en route to dissociation.

for the H + ketene channel to be more consistent with the velocity map imaging data than the G4 barrier height (42.2 kcal/mol), we used this new barrier height for the branching calculations in this study as well. The dashed green fit in Figure 6 to ketene from the unimolecular dissociation of vinoxy radicals was thus calculated from the vector sum of the velocities of vinoxy predicted to dissociate to H + ketene; the recoil velocity between H and ketene was calculated assuming an isotropic angular distribution and the secondary recoil translational energy distribution, P(E_T,2°), shown in Figure 8. Although we assumed in the previous study that the ketene

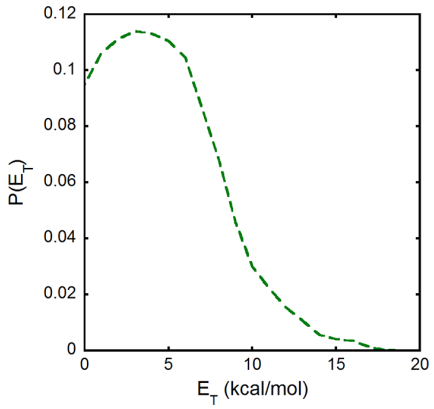

Figure 8. Product recoil kinetic energy distribution for the unimolecular dissociation of the vinoxy radical to H + ketene. The P(E_T,2°) is derived using an isotropic angular distribution by forward convolution fitting of the signal under the dashed green fit in the m/z = 42 (CH_2CO^+) TOF spectrum in Figure 6.

fragments receive negligible recoil from the secondary dissociation because ketene is much heavier than the H atom cofragment, this assumption is not appropriate for ketene from slower-moving vinoxy radicals. In this case, the secondary recoil imparted to the fragments is significant compared to the velocity imparted in the primary dissociation. This gives an excellent fit to ketene product with neutral flight times slower than the peak at 38 μs. However, we were unable to fit all of the signal at short arrival times in the TOF spectrum to ketene from secondary dissociation of vinoxy. We therefore considered a contribution from stable ketene produced from HCl photoelimination similar to that observed in the velocity map imaging study. The fit corresponding to stable ketene from HCl elimination of chloroacetaldehyde is shown by the solid blue line in Figure 6 and was derived from the P(E_T) by the solid black line shown in Figure 2. This P(E_T) thus corresponds to the portion of the HCl photoelimination events that produces stable ketene products. By subtracting this portion from the total HCl photoelimination P(E_T), we get the predicted unstable portion shown by the dashed black line in Figure 2. While a majority of the dissociation events produced unstable ketene, there are events that produce stable ketene.

3.3. C−C Bond Fission. Evidence for C−C bond fission is given in the TOF spectra taken at m/z = 49 (CH_2Cl^+) shown in Figure 9. The experimental data are shown in red circles. Because we expected a portion of the formyl radicals to be formed with enough vibrational energy to undergo subsequent unimolecular dissociation due to its low barrier to dissociation, we determined the P(E_T) for all C−C bond fission events from the TOF spectrum taken at m/z = 49 (CH_2Cl^+). The fit corresponding to C−C bond fission is depicted by the solid orange line in Figure 9 and was derived from the P(E_T) shown in Figure 10. The P(E_T) peaks at 8 kcal/mol and has a tail that extends to about 45 kcal/mol. The other contribution to the TOF spectrum at m/z = 49 (CH_2Cl^+) is dissociation of clusters in the molecular beam, which is shown by the solid purple line. It was not possible to fit the TOF data with a single P(E_T), and we also expect to see signal at this mass from clusters based on the energetics of producing CH_2Cl^+ ions from chloroacetaldehyde monomers. Uncertainty in the amount of signal from clusters affects only the C−C bond fission P(E_T) in the range

DOI: 10.1021/acs.jpca.7b05318
J. Phys. Chem. A XXXX, XXX, XXX−XXX

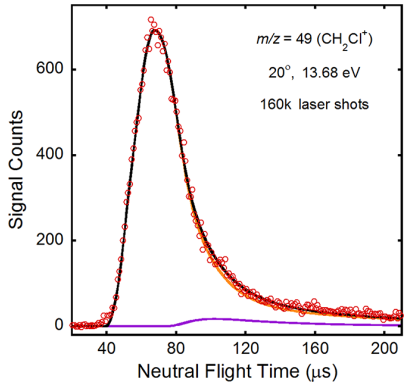

Figure 9. TOF spectrum taken at m/z = 49 (CH_2Cl^+) with a source angle of 20° and an ionization energy of 13.68 eV. Data are shown in red circles. Primary C−C bond fission is fit by the solid orange line using the $P(E_T)$ shown in Figure 10. The contribution attributed to photodissociation of clusters in the molecular beam is shown by the solid purple line.

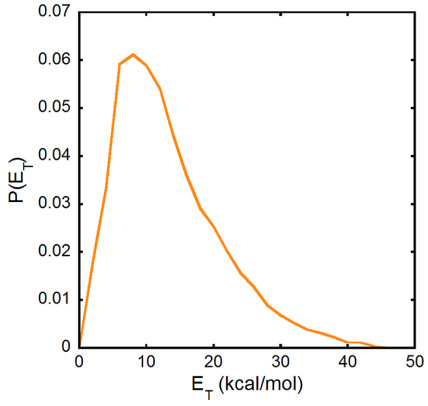

Figure 10. Photofragment recoil kinetic energy distribution for C−C bond fission in chloroacetaldehyde at 157 nm. The $P(E_T)$, peaking at 8 kcal/mol, is derived by forward convolution fitting of the signal at m/z = 49 (CH_2Cl^+) shown in Figure 9.

from 0−4 kcal/mol and thus introduces minimal error into our subsequent branching ratio calculations.

Figure 11 shows the TOF spectrum collected at m/z = 29 (HCO^+) with a source angle of 20° and ionization energy of 11.53 eV. The fit corresponding to momentum-matched cofragments of CH_2Cl is shown by the solid orange line; it peaks as expected at 50 μs. However, the integrated signal under the orange fits in the m/z = 29 TOF spectra show much less signal at HCO^+ than expected based on the relative photoionization cross sections.[13,25] We therefore suspect that the formyl radical undergoes unimolecular dissociation; indeed, the barrier to forming H + CO is only 16.5 kcal/mol.[26] The sharp and narrow peak at fast times is characteristic of dissociative ionization of stable vinoxy radicals. It is fit by the dashed gray line using the stable portion of the C−Cl bond fission $P(E_T)$ calculated from our branching calculations. We also included a contribution from dissociation of molecular clusters. However, there is still unfit signal at intermediate times (around 75 μs) between the cluster and C−C bond fission contributions. We were unable to identify the source of this signal.

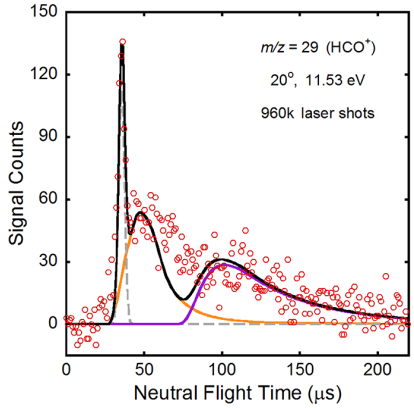

Figure 11. TOF spectrum taken at m/z = 29 (HCO^+) with a source angle of 20° and an ionization energy of 11.53 eV. Data are shown in red circles. The contribution from the momentum-matched cofragments to C−C bond fission is fit by the solid orange line using the $P(E_T)$ shown in Figure 10. Dissociative ionization of stable vinoxy to HCO^+ is shown as the dashed gray line and fit using the portion of the C−Cl bond fission $P(E_T)$, producing stable vinoxy radicals (shown by the dashed gray line in Figure 8). The fit shown by the solid purple line is the contribution attributed to photodissociation of clusters in the molecular beam. Because not all of the signal is accounted for by the fits, there is likely another source of m/z = 29.

3.4. Branching Ratios. To fully characterize the relative branching between the three primary photodissociation channels of chloroacetaldehyde, we calculated the branching ratio between the C−Cl bond photofission channel and both the HCl photoelimination and C−C bond photofission channels. For the branching ratio between the C−Cl bond fission channel and HCl photoelimination channel, we used the signal acquired at m/z = 35 (Cl^+) and m/z = 36 ($H^{35}Cl^+$) with a source angle of 10° and ionization energy of 13.68 eV. For the branching ratio between the C−Cl bond fission channel and C−C bond fission channel, we used the signal acquired at m/z = 35 (Cl^+) and m/z = 49 (CH_2Cl^+) with a source angle of 20° and ionization energy of 13.68 eV. (We used the spectra at a 20° source angle because m/z = 49 (CH_2Cl^+) showed a large beam-dependent signal at slower neutral flight times.) We first integrated the signal under the corresponding fits at each mass and calculated the ratio of these signals. The ratio of signals is given below as obs($^{35}Cl^+/H^{35}Cl^+$) and obs($^{35}Cl^+/CH_2Cl^+$), respectively. We then corrected these ratios for the expected signal based on kinematic corrections and Jacobian factors, TS($H^{35}Cl/^{35}Cl$) and TS($CH_2Cl/^{35}Cl$), as well as for the photoionization cross sections of the fragments (averaged over the bandwidth of the synchrotron radiation), σ_{X/X^+}. We used the photoionization cross section of Cl reported by Ruscic and Berkowitz[27] correcting for the lower cross section in the continuum beyond the ^1S_o threshold recommended by Berkowitz[28] based on subsequent studies. For HCl, we used the photoionization cross section reported by Frohlich and Glass-Maujean.[29] Because there are no prior reported photoionization cross sections for CH_2Cl, we used the relative cross section, $\sigma_{CH_2Cl/CH_2Cl^+}/\sigma_{Cl/Cl^+}$, determined in the photodissociation study by Scrape et al.[13] on dichloromethane done on the same instrument. We obtain

DOI: 10.1021/acs.jpca.7b05318
J. Phys. Chem. A XXXX, XXX, XXX−XXX

$$\frac{\Phi_{C-Cl}}{\Phi_{HCl}} = \text{obs}\left(\frac{^{35}Cl^+}{H^{35}Cl^+}\right)\text{TS}\left(\frac{H^{35}Cl}{^{35}Cl}\right)\left(\frac{\sigma_{HCl/HCl^+}}{\sigma_{Cl/Cl^+}}\right) = \left(\frac{75328}{13813}\right)\left(\frac{143732}{62697}\right)\left(\frac{16\text{ Mb}}{22.8\text{ Mb}}\right) = 8.8 \quad (5)$$

and

$$\frac{\Phi_{C-Cl}}{\Phi_{C-C}} = \text{obs}\left(\frac{^{35}Cl^+}{CH_2Cl^+}\right)\text{TS}\left(\frac{CH_2Cl}{^{35}Cl}\right)\left(\frac{\sigma_{CH_2Cl/CH_2Cl^+}}{\sigma_{Cl/Cl^+}}\right) = \left(\frac{19001}{30371}\right)\left(\frac{34137}{10780}\right)(1.17) = 2.3 \quad (6)$$

The combination of these two ratios yields total primary photodissociation branching fractions for C−Cl fission:HCl elimination:C−C fission of 0.65:0.07:0.28. Interestingly, C−C bond fission effectively competes with C−Cl bond fission in the primary photodissociation of chloroacetaldehyde at 157 nm. Any correction due to differing photofragment anisotropies is assumed to be negligible.

4.0. DISCUSSION

This study details the characterization of the primary photodissociation channels of chloroacetaldehyde at 157 nm and the reassessment of the subsequent dissociation dynamics of the vinoxy radicals produced by C−Cl bond fission. We first demonstrated that chloroacetaldehyde undergoes three primary dissociation channels: C−Cl bond fission, HCl photoelimination, and C−C bond fission. While C−Cl bond fission and HCl photoelimination have been observed in prior photodissociation studies of chloroacetaldehyde,[4,5] this study provides the first direct evidence of the C−C bond fission channel. Using the scattering data, we then estimated the branching ratios between the primary channels; we determined C−Cl bond fission and C−C bond fission to be major channels and HCl photoelimination to be a minor channel. We then investigated the possibility of stable ketene cofragments from HCl photoelimination contributing to the m/z = 42 TOF spectrum.

As in the velocity map imaging study,[5] the translational energy distribution for the C−Cl photofission channel (Figure 4) shows two main features: a low kinetic energy "shoulder" and a high kinetic energy peak at 42 kcal/mol. In the previous study, after accounting for the rotational energy imparted to the vinoxy radical, we concluded that the high kinetic energy component likely corresponds to vinoxy produced in the $\tilde{A}$ state following excitation to the S_3 state of chloroacetaldehyde, and the low kinetic energy component likely corresponds to vinoxy produced in the $\tilde{B}$ state following excitation to the S_4 state of chloroacetaldehyde. The present NSRRC data show additional signal on the high kinetic energy side of the C−Cl bond fission $P(E_T)$ that we did not observe in the velocity map imaging study, but the disagreement is within the joint resolution of the two apparatuses. While the goal of the previous study done at 157 nm was to investigate the unimolecular dissociation of vinoxy produced via C−Cl bond fission, we were unable to make any definite conclusions from the data collected at m/z = 15 and 42 in this work.

The C−C bond fission channel is of particular interest because it has not been directly observed before in the photodissociation of chloroacetaldehyde and it effectively competes with the C−Cl bond fission channel. Waschewsky et al.[6] and Alligood et at.[8] observed both C−Cl and C−C bond fission in their study on the photodissociation of chloroacetone at 308 and 193 nm, respectively. In both studies, they observed only C−C bond fission producing CH_2Cl and CH_3CO and detected no significant cleavage of the other C−C bond in the molecule. This is analogous to the C−C bond fission that occurs in chloroacetaldehyde, suggesting that the presence of the methyl group does not significantly affect the dynamics of chloroacetone as compared to that of chloroacetaldehyde. The branching ratio between these two primary dissociation channels was also calculated at both photodissociation wavelengths. At 308 nm, the branching ratio between C−Cl bond fission and C−C bond fission was 4.6:1;[6] and at 193 nm, the branching ratio was 11:1.[8] So, C−C bond fission can effectively compete with C−Cl bond fission in the photodissociation of chloroacetone.

In this study, the translational energy distribution for the C−C bond fission channel peaks at 8 kcal/mol, which suggests a small exit barrier to the dissociation. Compared to the other photodissociation pathways of chloroacetaldehyde at 157 nm, the C−C bond fission $P(E_T)$ has the smallest range of recoil translational energies (0−40 kcal/mol). These features are similar to the C−C bond fission channel observed in the photodissociation of chloroacetone at 193 nm;[8] however, the C−C bond fission $P(E_T)$ derived in that study peaks at a lower E_T (∼6 kcal/mol) and only ranges from 0−14 kcal/mol. In contrast to the chloroacetone study at 193 nm, we also report a smaller branching ratio between C−Cl bond fission and C−C bond fission. Because chloroacetaldehyde and chloroacetone have the same chromophores and same structure (with the exception of a methyl group in place of the aldehydic H atom), we expect the photodissociation dynamics of the two molecules to be quite similar to one another. Assuming the branching between C−Cl bond fission and C−C bond fission in chloroacetaldehyde at 193 nm is similar to that of chloroacetone, we see more branching to C−C bond fission at the higher photon energy of 157 nm.

Because two of the singlet excited states of chloroacetaldehyde in the vicinity of the excitation energy (S_2 and S_3) are repulsive along the C−Cl bond in the Franck−Condon region, we expect C−Cl bond fission to be the dominant channel. One singlet state, S_4, shows a well in the Franck−Condon region but is repulsive in the C−Cl bond at larger C−Cl internuclear distances. The observation of C−C bond fission suggests that the dynamics, perhaps via intersystem crossing, accesses a region of an excited state from which C−C bond fission can occur. Lucazeau and Sandorfy[11] suggested that predissociation of the excited states with Rydberg character in the Franck−Condon region in the region from 55 000 to 73 000 cm^{-1} by states with repulsive $n \rightarrow \sigma^*$ character might explain the diffuse character of the VUV absorption spectrum for chloroacetaldehyde. In comparison to the photodissociation of chloroacetone, Shen et al.[30] ran theoretical trajectories to investigate the observed selectivity of the C−C bond fission channels in the photodissociation of chloroacetone at 308 nm. They found that the effectiveness of the nonadiabatic $S_1 \rightarrow S_0$ transition in the vicinity of the barriers to each C−C bond fission channel was consistent with the selectivity. However, they were certain that the C−C bond fission did not ultimately occur on the ground-state singlet surface based on the experimentally determined $P(E_T)$ for the process. At 308 nm, S_0 and S_1 were the only singlets states energetically accessible to chloroacetone, which suggests that the C−C bond fission may occur instead on a triplet state. On the basis of time-dependent density functional

DOI: 10.1021/acs.jpca.7b05318
J. Phys. Chem. A XXXX, XXX, XXX−XXX

theory calculations, there may be a possible route to C−C bond fission along the T_1 state, which rises to a barrier and then falls as the C−C bond is stretched. At an excitation of 308 nm, the T_1 state is energetically accessible to chloroacetone, and the same is true of chloroacetaldehyde. Therefore, it is possible that the C−C bond fission occurs on this state following intersystem crossing from the S_1 state. For this state to be responsible for the observed C−C bond fission in the photodissociation at 157 nm, there must be an effective intersystem crossing process to the T_1 state. Comprehensive dynamics studies on the coupled singlet and triplet states would help elucidate the excited-state dynamics of chloroacetaldehyde and the branching fractions determined in this study. While HCl photoelimination is a minor channel, the relative amount of those dissociation events compared to C−Cl bond fission is calculated to be larger in this 157 nm study as compared to that calculated in the previous study at 193 nm done by Miller et al. Interestingly, this $P(E_T)$ peaks near the same recoil kinetic energy (E_T = 8 kcal/mol) as that measured for HCl photoelimination by Miller et al. in the photodissociation of chloroacetaldehyde at 193 nm; however, they do not see as many photodissociation events with higher translational energies. Because the photon energy is higher in our study, we have more energy in the system that can be converted into translation.

While Miller et al. were unable to characterize the portion of ketene cofragments from HCl photoelimination that undergo unimolecular dissociation, we were able to show that the portion of the HCl photoelimination $P(E_T)$ that corresponds to events producing stable ketene is quite small when 2-chloroacetaldehyde is photodissociated at 157 nm. This is consistent with our conclusion that HCl photoelimination did not significantly contribute to the m/z = 42 data from our previous velocity map imaging study. To form stable ketene cofragments, the HCl must be produced with significant vibrational energy following the dissociation. While we could not characterize the internal energy of the HCl fragments directly, the stable portion of the HCl photoelimination $P(E_T)$ shown in Figure 2 suggests that when E_T = 44 kcal/mol, the ketene fragments have less than 84 kcal/mol of internal energy (the barrier to dissociation of ketene to CH_2 + CO). The momentum-matched HCl would thus have greater than 47.6 kcal/mol, which corresponds to roughly 6 quanta in vibration (assuming rotational energy is negligible). When the HCl photoelimination partitions less than 44 kcal/mol to relative kinetic energy, some of the ketene dissociates to CH_2 + CO, leaving the HCl with less than 6 quanta in vibration. A complementary study on the characterization of the vibrational and rotational energy distributions of HCl products, resolved by recoil velocity, would provide information about the internal energy available to the ketene cofragments, allowing a more precise determination of the portion of the HCl elimination $P(E_T)$ that produces stable ketene cofragments. This contribution is important because it affects the analysis of the m/z = 42 spectrum with regard to the onset of the H + ketene channel in the dissociation of vinoxy radicals.

While we assumed that the HCl photoelimination proceeds via a four-center mechanism, thus producing ketene as a cofragment, a three-center mechanism is also possible, which would produce the HCCHO biradical cofragment. Photoelimination of hydrogen halides is often observed in the photodissociation of organohalides, and this process has been shown to proceed via three-center, four-center, or roaming-type mechanisms.[31−36] Similar systems have shown evidence of both mechanism types; however, we cannot confirm if we observe the three-center mechanism. On the basis of electronic structure calculations (see Supporting Information), the lowest barrier on the ground state PES of the HCCHO radical is isomerization to ketene, where it can further undergo dissociation to CH_2 + CO as the ketene products do. This makes it difficult to confirm the presence of the HCCHO radical and evidence of the three-center mechanism. Prior studies have found that the vibrational and rotational energy distributions of the HCl product produced from the two mechanism types are generally different. Therefore, another benefit to further characterizing the internal energy distribution of the HCl products from photodissociation of chloroacetaldehyde would be to confirm the presence of two distinct mechanisms for HCl photoelimination.

Another interesting aspect about the scattering data for HCl photoelimination is the notable difference between the TOF spectra taken at m/z = 36 ($H^{35}Cl^+$) and at m/z = 38 ($H^{37}Cl^+$). We show the TOF spectra at m/z = 36 in the Supporting Information. The TOF spectra taken at m/z = 36 ($H^{35}Cl^+$) show faster signal that is dependent on the ionization energy used to collect the data. This signal is not observed in the TOF spectrum taken at m/z = 38 ($H^{37}Cl^+$). If the extra fast signal observed at m/z = 36 ($H^{35}Cl^+$) is from bleed in of the m/z = 37 (Cl^+) signal, then we would not expect to see the same signal in the m/z = 38 ($H^{37}Cl^+$) because there is no bleed in to that data from higher masses. Based on the resolution of the quadrupole, the maximum amount of bleed in from the m/z + 1 signal into the m/z signal is 10%, and the amount of signal observed at m/z = 37 (Cl^+) is not enough to account for all of the fast signal in Figure S.7 in the Supporting Information. One possibility is that HCl photoelimination occurs via two distinct mechanisms which experience different isotope effects. As for the dependence on the ionization energy, HCl produced in different vibrational energy states may be more efficiently ionized at one ionization energy over the other.

5.0. CONCLUSION

In this study, we further characterized the primary photodissociation pathways of chloroacetaldehyde and observed that chloroacetaldehyde undergoes C−Cl bond fission, HCl photoelimination, and C−C bond fission upon excitation at 157 nm. The C−C bond fission channel has not been directly observed before and competes with C−Cl bond fission based on our measured branching ratio. Because the singlet electronically excited states of chloroacetaldehyde accessed at 157 nm are either directly repulsive or predissociative along the C−Cl bond in the Franck−Condon region, the presence of the C−C bond fission channel suggests possible internal conversion/intersystem crossing. This result warrants further study of the dynamics on the excited-state PESs of chloroacetaldehyde. While HCl photoelimination is a minor channel, it is important to consider its contribution to the m/z = 42 data. We do observe signal in the m/z = 42 TOF spectrum that we attribute to stable ketene cofragments from HCl photoelimination, but the signal appears at early arrival times and so overlaps slightly with the signal from the unimolecular dissociation of the higher recoil kinetic energy vinoxy radicals. This is consistent with the assignment of the high kinetic energy ketene signal in the velocity map imaging data to stable ketene produced from HCl photoelimination. Because we detect stable ketene cofragment in both studies and the endoergicity of this primary channel is low, characterization of the internal energy distribution in the

DOI: 10.1021/acs.jpca.7b05318
J. Phys. Chem. A XXXX, XXX, XXX−XXX

photoproducts would be an interesting complementary study. This type of study could also be helpful in determining the mechanism of HCl photoelimination.

■ ASSOCIATED CONTENT

Supporting Information

The Supporting Information is available free of charge on the ACS Publications website at DOI: 10.1021/acs.jpca.7b05318.

(A) molecular beam speed distribution, (B) alternative fits to $m/z = 35$ and $m/z = 36$ TOF spectra using the C−Cl bond fission P(E_T) from the velocity map imaging study, (C) further details on the branching calculations, (D) critical points on the potential energy surface of the HCCHO radical, (E) calculation of branching ratios between the primary photodissociation channels using the C−Cl bond fission P(E_T) from the velocity map imaging study, and (F) isotope dependence of the HCl elimination TOF data (PDF)

■ AUTHOR INFORMATION

Corresponding Author

*E-mail: l-butler@uchicago.edu.

ORCID

Laurie J. Butler: 0000-0001-6965-3438

Notes

The authors declare no competing financial interest.

■ ACKNOWLEDGMENTS

This work was supported by the U.S. Army Research Laboratory and the U.S Army Research Office under Contract W911NF-14-1-0244 (L.J.B.). Synchrotron beam time and additional funding were provided by the National Synchrotron Radiation Research Center and Academia Sinica. We gratefully thank Mr. Wen-Jian Huang and Dr. Yi-Lun Sun for their assistance in maintaining and using the apparatus at the NSRRC. We also thank Dr. Matthew D. Brynteson for his assistance with data collection.

■ REFERENCES

(1) Tuazon, E. C.; Atkinson, R.; Winer, A. M.; Pitts, J. N. A Study of the Atmospheric Reactions of 1,3-Dichloropropene and Other Selected Organochlorine Compounds. *Arch. Environ. Contam. Toxicol.* **1984**, *13*, 691−700.

(2) Calvert, J. G.; Derwent, R. G.; Orlando, J. J.; Tyndall, G. S.; Wallington, T. J. *Mechanisms of Atmospheric Oxidation of the Alkanes*; Oxford University Press: New York, 2008.

(3) Starcke, J.; Zabel, F.; Elsen, L.; Nelsen, W.; Barnes, I.; Becker, K. H. *Physico-Chemical Behaviour of Atmospheric Pollutants*; Kluwer Academic Publishers: Dordrecht, 1990.

(4) Miller, J. L.; McCunn, L. R.; Krisch, M. J.; Butler, L. J.; Shu, J. Dissociation of the Ground State Vinoxy Radical and Its Photolytic Precursor Chloroacetaldehyde: Electronic Nonadiabaticity and the Suppression of the H + Ketene Channel. *J. Chem. Phys.* **2004**, *121*, 1830−1838.

(5) Lam, C.-S.; Adams, J. D.; Butler, L. J. The Onset of H + Ketene Products from Vinoxy Radicals Prepared by Photodissociation of Chloroacetaldehyde at 157 nm. *J. Phys. Chem. A* **2016**, *120*, 2521−2536.

(6) Waschewsky, G. C. G.; Kash, P. W.; Myers, T. L.; Kitchen, D. C.; Butler, L. J. What Woodward and Hoffman Didn't Tell Us: The Failure of the Born-Oppenheimer Approximation in Competing Reaction Pathways. *J. Chem. Soc., Faraday Trans.* **1994**, *90*, 1581−1598.

(7) Kitchen, D. C.; Myers, T. L.; Butler, L. J. Determination of Absolute Product Branching Ratios in Mass Spectrometric Experiments: Detecting Acetyl Radicals at CH_2CO^+. *J. Phys. Chem.* **1996**, *100*, 5200−5204.

(8) Alligood, B. W.; Fitzpatrick, B. L.; Szpunar, D. E.; Butler, L. J. Chloroacetone Photodissociation at 193 nm and the Subsequent Dynamics of the $CH_3C(O)CH_2$ Radical - An Intermediate Formed in the OH + Allene Reaction En Route to CH_3 + Ketene. *J. Chem. Phys.* **2011**, *134*, 054301.

(9) Nelson, L.; Shanahan, I.; Sidebottom, H. W.; Treacy, J.; Nielsen, O. J. Kinetics and Mechanism for Oxidation for 1,1,1-Trichloroethane. *Int. J. Chem. Kinet.* **1990**, *22*, 577−590.

(10) Burkholder, J. B.; Gilles, M. K.; Gierczak, T.; Ravishankara, A. R. The Atmospheric Degradation of 1-Bromopropane ($CH_3CH_2CH_2Br$): The Photochemistry of Bromoacetone. *Geophys. Res. Lett.* **2002**, *29*, 1822−1825.

(11) Lucazeau, G.; Sandorfy, C. On the Far-Ultraviolet Spectra of Some Simple Aldehydes. *J. Mol. Spectrosc.* **1970**, *35*, 214−231.

(12) NIST. Chemistry WebBook. http://webbook.nist.gov/chemistry/.

(13) Scrape, P. G.; Xu, R.; Adams, J. D.; Lee, S.-H.; Butler, L. J. A Measurement of the Photoionization Cross Section of CH_2Cl via Photofragment Translational Spectroscopy of Dichloromethane. Submitted to *Chem. Phys. Lett.*, **2017**

(14) Ratliff, B. J.; Alligood, B. W.; Butler, L. J.; Lee, S.-H.; Lin, J. J. Product Branching from the CH_2CH_2OH Radical Intermediate of the OH + Ethene Reaction. *J. Phys. Chem. A* **2011**, *115*, 9097−9110.

(15) Lin, J. J.; Chen, Y.; Lee, Y. Y.; Lee, Y. T.; Yang, X. Photodissociation Dynamics of CH_3Cl at 157.6 nm: Evidence for CH_2 (X^3B_1/a^1A_1) + HCl Product Channels. *Chem. Phys. Lett.* **2002**, *361*, 374−382.

(16) Lee, Y. T.; McDonald, J. D.; LeBreton, P. R.; Herschbach, D. R. Molecular Beam Reactive Scattering Apparatus with Electron Bombardment Detector. *Rev. Sci. Instrum.* **1969**, *40*, 1402−8.

(17) Zhao, X., modified by Myers, J. D. *CMLAB2*, version 6/93, an interactive version built on the original cmlab2 program. Ph.D. Dissertation, University of California, 1988.

(18) Curtiss, L. A.; Redfern, P. C.; Raghavachari, K.; Pople, J. A. Gaussian-3X (G3X) Theory: Use of Improved Geometries, Zero-Point Energies, and Hartree-Fock Basis Sets. *J. Chem. Phys.* **2001**, *114*, 108−117.

(19) Curtiss, L. A.; Redfern, P. C.; Raghavachari, K. Gaussian-4 Theory. *J. Chem. Phys.* **2007**, *126*, 084108.

(20) Frisch, M. J.; Trucks, G. W.; Schlegel, H. B.; Scuseria, G. E.; Robb, M. A.; Cheeseman, J. R.; Scalmani, G.; Barone, V.; Mennuci, B.; Petersson, G. A.; et al. *Gaussian 09*, revision A.02; Gaussian, Inc.: Wallingford, CT, 2009.

(21) Adams, J. D. Product Branching in the Photodissociation of Chloroacetaldehyde and the Incorporation of Angular Momentum in Statistical Predictions of Product Branching. Ph.D. Dissertation, The University of Chicago, Chicago, IL, 2017.

(22) Ratliff, B. J.; Tang, X.; Butler, L. J.; Szpunar, D. E.; Lau, K.-C. Determining the $CH_3SO_2 \rightarrow CH_3 + SO_2$ Barrier from Methylsulfonyl Chloride Photodissociation at 193 nm Using Velocity Map Imaging. *J. Chem. Phys.* **2009**, *131*, 044304.

(23) Alligood, B. W.; FitzPatrick, B. L.; Glassman, E. J.; Butler, L. J.; Lau, K.-C. Dissociation Dynamics of the Methylsulfonyl Radical and Its Photolytic Precursor CH_3SO_2Cl. *J. Chem. Phys.* **2009**, *131*, 044305.

(24) Scrape, P. G.; Roberts, T. D.; Lee, S.-H.; Butler, L. J. Dissociation Pathways of the CH_2CH_2ONO Radical: NO_2 + Ethene, NO + Oxirane, and a Non-Intrinsic Reaction Coordinate HNO + Vinoxy Pathway. *J. Phys. Chem. A* **2016**, *120*, 4973−4987.

(25) FitzPatrick, B. L.; Alligood, B. W.; Butler, L. J.; Lee, S.-H.; Lin, J. J. Primary Photodissociation Pathways of Epichlorohydrin and Analysis of the C−C Bond Fission Channels From an O(^{3}P)+Allyl Radical Intermediate. *J. Chem. Phys.* **2010**, *133*, 094306.

(26) Werner, H.-J.; Bauer, C.; Rosmus, P.; Keller, H.-M.; Stumpf, M.; Schinke, R. The Unimolecular Dissociation of HCO: Oscillations of

DOI: 10.1021/acs.jpca.7b05318
J. Phys. Chem. A XXXX, XXX, XXX−XXX

Pure CO Stretching Resonance Widths. *J. Chem. Phys.* **1995**, *102*, 3593−3611.
(27) Ruscic, R.; Berkowitz, J. Photoionization of Atomic Chlorine. *Phys. Rev. Lett.* **1983**, *50*, 675−678.
(28) Berkowitz, J. *Atomic and Molecular Photoabsorption: Absolute Total Cross Sections*; Academic: San Diego, CA, 2002.
(29) Frohlich, H.; Glass-Maujean, M. Photoabsorption, Photodissociation, and Photoionization Cross Sections of HCl. *Phys. Rev. A: At., Mol., Opt. Phys.* **1990**, *42*, 1396−1404.
(30) Shen, L.; Liu, L.; Cao, J.; Fang, W.-H. Insights into Mechanistic Photodissociation of Chloroacetone from a Combination of Electronic Structure Calculation and Molecular Dynamics Simulation. *J. Chem. Phys.* **2011**, *135*, 194305.
(31) Lin, J. J.; Chen, Y.; Lee, Y. Y.; Lee, Y. T.; Yang, X. Photodissociation Dynamics of CH_3Cl at 157.6 nm: Evidence for $CH_2(\tilde{X}^3B_1/\tilde{a}^1A_1)$ + HCl Product Channels. *Chem. Phys. Lett.* **2002**, *361*, 374−382.
(32) Lin, S.-R.; Lin, S.-C.; Lee, Y.-C.; Chou, Y.-C.; Chen, I.-C.; Lee, Y.-P. Three-Center versus Four-Center HCl-elimination in Photolysis of Vinyl Chloride at 193 nm: Bimodal Rotational Distribution of HCl ($v \leq 7$) Detected with Time-Resolved Fourier-Transform Spectroscopy. *J. Chem. Phys.* **2001**, *114*, 160−168.
(33) Saha, A.; Kawade, M.; SenGupta, S.; Upadhyaya, H. P.; Kumar, A.; Naik, P. D. Photodissociation Dynamics of Benzoyl Chloride at 235 nm. *J. Phys. Chem. A* **2014**, *118*, 1185−1195.
(34) Lee, P.-W.; Scrape, P. G.; Butler, L. J.; Lee, Y.-P. Two HCl-Elimination Channels and Two CO-Formation Channels Detected with Time-Resolved Infrared Emission upon Photolysis of Acryloyl Chloride [$CH_2CHC(O)Cl$] at 193 nm. *J. Phys. Chem. A* **2015**, *119*, 7293−7304.
(35) Brynteson, M. D.; Womack, C. C.; Booth, R. S.; Lee, S.-H.; Lin, J. J.; Butler, L. J. Radical Intermediates in the Addition of OH to Propene: Photolytic Precursors and Angular Momentum Effects. *J. Phys. Chem. A* **2014**, *118*, 3211−3229.
(36) Booth, R. S.; Brynteson, M. D.; Lee, S.-H.; Lin, J. J.; Butler, L. J. Further Studies into the Photodissociation Pathways of 2-Bromo-2-nitroproane and the Dissociation Channels of the 2-Nitro-2-propyl Radical Intermediate. *J. Phys. Chem. A* **2014**, *118*, 4707.

DOI: 10.1021/acs.jpca.7b05318
J. Phys. Chem. A XXXX, XXX, XXX−XXX